Characterization of aluminum alloy-epoxy bonded joints with nanofibers obtained by electrospinning

Characterization of aluminum alloy-epoxy bonded joints with nanofibers obtained by electrospinning

D. Cocchi[1], F. Musiari[2], T. M. Brugo[1], A. Pirondi[2], A. Zucchelli[1], F. Campanini[3], E. Leoni[4], L. Mazzocchetti[4]

[1]*Dipartimento di Ingegneria Industriale, Alma Mater Studiorum - Università di Bologna*
viale del Risorgimento 2, 40136 Bologna, Italy

[2]*Dipartimento di Ingegneria e Architettura, Università di Parma*
Parco Area delle Scienze 181/A, 43124 Parma, Italy

[3]*ELANTAS Europe Srl*
Strada Antolini 1 loc. Lemignano, 43044 Collecchio, Italy

[4]*Dipartimento di Chimica Industriale, Alma Mater Studiorum - Università di Bologna*
viale del Risorgimento 4, 40136 Bologna, Italy

Abstract

In previous works, the authors showed that nylon nanofibers in the form of a random mat (nanomat) obtained by electrospinning can be used in bonded joints, where they may also work as adhesive carrier. In those works, the setup of the bonding procedure started from a low-viscosity epoxy resin for hand layup in order to facilitate wetting of the nanomat, then a medium viscosity, two-component, unfilled epoxy adhesive was employed as an intermediate development step towards the addition of the nanomat to a high-viscosity, high strength, two-component epoxy adhesive system. The present work is therefore aimed at analysing the performance of an epoxy adhesive for structural bonding, modified with the addition of a nylon nanomat generated by electrospinning. The adhesive is mixed and air bubbles are evacuated, then the nanomat is immersed in the adhesive, gently squeezed through two adjacent drums, counter-rotating at a given distance, in order to eliminate excess adhesive and to calibrate the wet nanomat thickness. The wet nanomat strip is finally placed between AA 6082-T4 adherents and let to consolidate to obtain Double Cantilever Beam (DCB) bonded specimens. Fracture tests are performed and the mode-I fracture toughness with and without the nanomat is compared.

Contact: Prof. Alessandro Pirondi, alessandro.pirondi@unipr.it

Keywords: nanomaterials**,** bonding reinforcement, fracture, aluminium and alloys

Nomenclature

a	crack length
A	cross-section of the adherent
b	width of the specimen
g	distance from load axis of CMOD measurement point
E	Young's modulus of the adherent
E_a	Young's modulus of the adhesive
G_I	Mode I strain energy release rate
G_{IC}	fracture toughness
h	thickness of the adherent
J	area moment of inertia of the adherent
k	elastic foundation stiffness [32]
P	force
t	thickness of the bonding interface
δ'	Crack Mouth Opening Displacement (CMOD)
λ_σ	length scale of the stress distribution in a DCB joint [32]
ν_a	Poisson's coefficient of the adhesive

1. Introduction

Structural adhesive bonding is increasingly used in joining multi-material, lightweight structures with high strength to weight ratios [1]. When looking among structural adhesives, epoxies are found to exhibit high modulus, high strength and good performance at intermediate to high temperatures. On the other hand, if taken alone they fail in a relatively brittle fashion, therefore they are generally toughened by adding, for instance, organic (rubber-like), inorganic (mineral, ceramic) particles or chopped fibres [2]. The review work of [3] quoted nanoreinforcement as an effective way to improve mechanical properties of the adhesive. However, they also concluded that it is difficult to obtain a unique influence from nanoparticles because this depends considerably on the manufacturing procedure. Epoxy adhesive reinforced with alumina nanospheres and nanorods prepared in [4] by in-situ polymerisation technique showed a significant effect on shear strength as well as opening mode

fracture toughness. The addition of Carbon Nanotubes (CNTs) as nanofillers can also improve stiffness, strength, fracture toughness and electrical conductivity [5]-[12]. However, concerning strength and fracture toughness, the results of those studies showed that both an increase or a decrease was possible depending on the CNT content and type, surface treatment, dispersion, testing methodology and temperature. In [11] the addition of graphene nanoplatelets, graphene oxide nanoplatelets and fullerene C60, beside carbon nanotubes, to three different types of epoxy ahesive was studied showing that all this doping nanostructures can improve the stress-strain capacity of the adhesives.

It has been shown in [13] that the use of polymeric, composite, or ceramic nanofibers yields a reinforcement more effective than with conventional fibres. In this sense, nanofibers generated by electrospinning provide a simple and versatile method for the reinforcement of composite laminates against delamination, by simply interleaving a randomly-oriented nanofiber mat (nanomat) between adjacent plies. This yields a ply-to-ply bridging that increases the delamination strength of the composite laminate, as shown several times during the last decade (see [14]-[17]). Unidirectional (UD) carbon/epoxy composite laminates exhibited fracture toughness improvements up to 156% and 69% for Mode I and Mode II, respectively, [18]. Unidirectional glass/epoxy composite laminates with interleaved Nylon 6,6 nanofibers showed also [19] a relevant increase of both Mode I and Mode II fracture toughness. Epoxy-dissolvable thermoplastic phenoxy interleaves yielded a pronounced toughening of epoxy resin [20]. This toughening strategy was also confirmed in [21], where a cylindrical woven copper wire mesh with polytetrafluoroethylene strips introduced at regular intervals along the bondline caused large-scale bridging of the crack. Aligned electrospun nanofibrous structures gave a strong effect of the nanofiber orientation in [22], but always leading to an increase of fracture toughness due to crack bridging. Improvements were detected also in the case of fatigue delamination [23]. A CNT-embedded PVB solution was directly electrospun onto carbon fiber prepregs in [24] in order to ease the manufacturing of interleaved composite laminates, reporting an almost 2-fold increase in G_C compared to non-interlayered laminates associated to the PVB/CNTs nanofibrous interlayers.

In adhesive bonding, electrospun nanomats can be potentially used as an alternative, for example, to conventional glass fibre mats employed in pre-cured, supported adhesive films, yielding at the same time a crack toughening. This application of electrospun nanofibers has still received little attention, with only a few papers published [25]-[28]. PolyAcryloNitrile (PAN) nanofibers were laid by direct electrospinning on the 2K epoxy adhesive (UHU plus Endfest 300) on the surfaces of 7075-T651 aluminium substrates [27], obtaining a two-fold increase of the fracture toughness with respect to the neat adhesive, though this latter was quite low (av. value G_c = 0.11 N/mm over 30 mm of crack

propagation). In [28], PVA electrospun nanofiber mats were placed before curing between single-lap and DCB joints adherents bonded with an epoxy adhesive. An increase of 13.50% of shear strength was found, while mode I fracture toughness was about twice the neat adhesive. In these works however, no one attempted to develop a pre-preg nanomat to facilitate the application of the nanofibers, since the nanomat is generally difficult to handle due to the small stiffness and the tendency to fold.

The potential of electrospun nylon nanofibrous mats to carry the adhesive and reinforce the joint, has been evaluated by the authors in previous works [29], [30]. The setup of the bonding procedure started from a low-viscosity epoxy resin for hand layup [29] in order to facilitate wetting of the nanomat, then a medium viscosity, two-component, multi-purpose unfilled epoxy adhesive was employed as an intermediate development step in [30] towards the addition of the nanomat to a high-viscosity, high strength, two-component epoxy adhesive system. However, in those works the joint exhibited limited adhesion and a fracture toughness lower that typical of epoxy adhesive systems, therefore the present work is aimed at manufacturing a structural epoxy adhesive joint with a nylon nanomat generated by electrospinning as a reinforcing web. The adhesive is mixed and air bubbles are evacuated, then the nanomat is immersed in the adhesive, gently squeezed through two adjacent drums, counter-rotating at a given distance, in order to eliminate excess adhesive and to calibrate the wet nanomat thickness. The wet nanomat strip is finally placed between AA 6082-T4 adherents and let to consolidate to obtain Double Cantilever Beam (DCB) bonded specimens. Fracture tests are performed and the mode-I fracture toughness with and without the nanomat is compared.

2. Experimental methodology

2.1. Polymeric nanofibrous mats

A nanomat, named EM252, is manufactured out of pellets of nylon 6,6 Zytel E53 NC010 (DuPont de Nemours Italiana S.r.l., Cernusco Sul Naviglio (MI), Italy). Alike previous works, the EM252 is obtained by dissolving 13% by weight of nylon 6,6 in a 10:60:30 by volume trifluoracetic acid / formic acid / chloroform solution (Sigma Aldrich – Italy, Milan). The choice of nylon was done for coherence with previous works [29] and [30], though the nylon/epoxy adhesion is generally poor, a reinforcing mechanism related to fibre bridging was demonstrated to exist in [15].

The solution is injected in a needle, kept under high voltage by a power supply, and then electrospun in the form of a 400x300 mm^2 foil. In the first millimetres after the needle, when the forces generated by an electric field between the needle and the electric ground overcome the surface tension of the solution, the solvent undergoes flash evaporation and the polymerization of nylon occurs. The

filament is collected over a rotating drum kept at zero electric potential. A random mat is formed as the filament is whirled around by electric forces, Figure 1. The process parameters are summarized in Table 1.

The thickness of the nanomat is included in the range between 50 and 82 μm, that is the average value detected along the nanomat strip by a digital indicator (ALPA, Pontoglio (BS), Italy) with a 0.65 N preload, resolution of 1 μm, max error of 4 μm and repeatability of 2 μm, while the nanofibers are assumed to have a diameter of 150±20 nm alike previous works ([29], [30]), since the electrospinning process parameters are the same. A thickness of the nanomat lower than that of those works is instead chosen in order to facilitate the wetting of the nanomat by the adhesive, that has a viscosity higher than the resins used in [29], [30].

One hour before adhesive application, the nanomat is placed for 15 min under vacuum and then heated in oven at 40°C for at least 30min, in order to eliminate humidity and solvent residues.

2.2. Adherents

A 6082-T4 aluminium plate is cut and machined in order to obtain 100(l)x10(b)x5(h) mm^3 adherents. This non-standard, small size has been selected for the sake of an easier manipulation of the nanomat, especially after the wetting in the adhesive. The surface to be bonded undergoes the following preparation sequence, developed after a careful literature survey:

1. polishing;
2. cleaning and degreasing;
3. pickling with alkaline solution (100g/L NaOH) at 60°C for 1 min;
4. rinsing and sonication in water;
5. wiping with blotting paper and cleaning;
6. P2-etching at 65°C for 12min according to ASTM D2651-01;
7. repeating of steps 4 and 5;
8. 5 hours self-passivation in air;
9. 15 min under vacuum 1h before bonding;
10. oven heating at 40°C for 30min

Chemical etching was done instead of sandpapering/sandblasting because of the potential in yielding higher adhesion and to avoid the formation of adhesive pockets close to the surface as detected in [29]. The results in terms of surface morphology are shown in Figure 2a-b. One can see the distribution of pit sizes, ranging about 1-10 μm and where smaller pits develop also inside larger ones as a result of the etching process. The value of roughness, measured with a Taylor-Hobson CCI non-contact profilometer (resolution 340 nm longitudinal, 1 nm vertical; Taylor-Hobson Ltd, Leicester,

UK) is Ra = 0.91 μm instead of Ra = 0.45 μm obtained in [30].

2.3. Specimen fabrication

The adhesive is supplied by ELANTAS (ELANTAS Europe srl, Collecchio (PR), Italy). Bulk properties from the datasheet of the supplier are summarized in Table 2. Preliminary tests aimed at evaluating qualitatively the impregnation were done in [30], where the two parts were mixed in a glass beaker, the mixture was then poured in a large bowl where the nanomat was immersed for a few minutes in order to fully wet (full wetting = transparency of the mat when picked up and exposed to light) and the wet nanomat strip was cured in a vacuum bag following the cycle in Table 2 without placing it between adherents. The cured epoxy + nanomat strip was examined optically on the outer surface to look for entrapped air bubbles ("External surface" in Figure 3), then it was broken manually and examined at the SEM ("Rupture surface" in Figure 3). From the SEM images, it is evident the presence of large air bubbles, therefore in this work a new procedure has been developed, the consists of the following steps:

1. pour the two parts of the adhesive in beaker;
2. gently mix under vacuum;
3. drip the mixed adhesive on the nanomat strip and distribute using a spatula;
4. wait for absorption of the adhesive into the nanomat until it becomes transparent;
5. calibrate the wet nanomat through two motorized, counter-rotating drums (Figure 4);

A so called ‘virgin’ (V) and a nanomodified (N) joints are manufactured, where in the latter the adherents are bonded with the addition of the nanomat. The N joints are manufactured before the V ones in order to evaluate the bondline thickness after curing. The nanomat is wet according to the procedure described previously, placed on one adherent, then the second adherent closes the joint. The bonding is done in a template where the specimens are left until consolidation, Figure 5. A 35 mm-long defect is obtained by inserting a PTFE foil into the nanomat before wetting, according to the procedure described in [30] and illustrated in Figure 6.

The specimens are subjected to a dead load (average pressure generated equal to 50 kPa) in order to evacuate the adhesive in excess and then cured in air according to the supplier prescriptions. The choice of curing in air is related to the observation that the application of vacuum in the case of V specimen promoted the suction of the not yet cured adhesive.

After curing, the specimens of the N type are removed from the template and the effective thickness of the bondline is measured by an optical microscope at three equally spaced points on both sides. The thickness varies from 58 to 95 μm, that is with a slight increase with respect to the dry nanomat due to the presence of the adhesive. In order to avoid the dependency of fracture toughness on

bondline thickness [31], the V specimens are manufactured with spacers at the extremities that result a thickness in the same range of the N ones.

2.4. DCB testing

Tests are performed under displacement control at a constant crosshead velocity on a servo-hydraulic MTS 810 testing machine equipped with a 3 kN load cell and the Crack Mouth Opening Displacement (CMOD), δ' (Figure 7), is evaluated by a clip gage. The crack length is calculated from the specimen compliance using a beam on elastic foundation concept that considers the out of plane deformation of the adhesive layer and the rotation at the crack tip [32], modified to account for the distance of the CMOD measurement point from the loading axis (g in Eq. 1) and for the effect of shear on the deformation of the cantilever (rightmost term in Eq. 1)

$$\frac{\delta'}{P} = 2\left[\frac{2\lambda_\sigma}{k}(1+\lambda_\sigma a) + (a+g)\frac{2\lambda_\sigma{}^2}{k}(1+2\lambda_\sigma a) + \frac{a^3}{3EJ} + g\frac{a^2}{2EJ}\right] \quad (1)$$

where λ_σ and k are

$$\lambda_\sigma = \sqrt[4]{\frac{6}{h^3 t}\frac{E_a}{E\left(1-\nu_a^2\right)}} \quad (2)$$

$$k = \frac{2b}{t}\frac{E_a}{(1-\nu_a{}^2)} \quad (3)$$

The strain energy release rate G is:

$$G = \frac{P^2 a^2}{bEJ}\left(1+\frac{1}{\lambda_\sigma a}\right)^2 \quad (4)$$

The Young's modulus of 6082-T4 is considered to be E = 70 GPa, a typical value for aluminum alloys. Concerning the adhesive, the Young's modulus, E_a, is taken equal to the average value of the flexural modulus indicated in the supplier datasheet (1800 MPa, see Table 2) and $\nu_a = 0.4$ as common in epoxies. Since the fibre volume fraction in the nanomat is a just a few percent, it causes a negligible change of Young's modulus with respect to the one of the adhesive, hence the Young's modulus of the adhesive+nanomat is the same of the adhesive alone.

3. Results and discussion

The Force vs. CMOD relative to both the virgin (V) and nanomodified (N) specimens are presented in Figure 8a and Figure 8b, respectively, in order to have a more clear overview of the trends; loading-unloading steps for the evaluation of the compliance are also reported. Both for the V and the N joints the behavior is smooth, indicating a progressive growth of the crack, i.e. without jumps and following arrests. The peak forces of the V joints are lower than those of the N ones, from which a higher fracture toughness of nanomodified joints can be foreseen. For values of CMOD greater than 2 mm the overall trends of the N and V joints get closer, hence the force shows a sharper decrease in the case of N joints; therefore in order to say if a difference in terms of fracture toughness persists the whole R-curve presented in Figure 9 has to be examined. Differently from what the examination of the overall Force-CMOD data indicate, the N joints that start from values of G_c comparable or lower than the V ones (average value 0.23 N/mm against 0.26 N/mm) that may imply a similar crack initiation mechanism. From the visual inspection of the fracture surfaces in two selected cases, one N (Figure 10a) and one V (Figure 10b), it is indeed not possible to distinguish a different failure mechanism, that is characterized by a failure at or close to the interface despite the etching treatment of the aluminum adherents and the low thickness of the bondline. This mechanism may justify also the relatively moderate value of fracture toughness for a structural adhesive. On the other hand, with increasing crack propagation the fracture toughness of N joints increase more rapidly than that of V joints, meaning that some kind of toughening mechanism related to the nanofibers develops. This is corroborated, for crack propagations in the range 4-8 mm, by the fact that the scatterbands of N and V joints, represented in Figure 9 by the average value +/- one-half standard deviation, are not overlapped. The fracture surfaces in Figure 10a-b are characterized in both cases by frequent crack path deviations from close to one adherent to the other one, with a balance of the adhesive left on the two surfaces. Only in the case of N joints, some adhesive seems to be left also on the brighter side, that may justify the higher fracture toughness with respect to the V ones. In the case of specimen N3 (Figure 11a), the crack path deviations were less frequent, therefore the value of G_c, initially higher than V joints, decreased with crack propagation approaching the one of the V3 joint, where a similar crack path was detected, Figure 11b. Hence, the joints that performed better are those with more frequent crack path deviations because it implies more energy dissipation.

In order to understand better if N joints do have some residue of adhesive on the brighter adherent and why they perform a little bit better than V joints, the fracture surfaces were examined at the ESEM. In Figure 12a (see Figure 10 for the position where pictures are taken) a mechanism is revealed, that is very similar to the one identified in [30] in the case of a nanomat-reinforced, general purpose, non-structural epoxy adhesive: the crack did not progress into the nanomat (see the pickled

aspect of the naked aluminium surface due to P2 etching) but ripples of adhesive+nanomat are left in correspondence of deeper grooves on the surface that act as anchor points. A higher magnification picture of the same region is reported in Figure 12b, that highlights the presence of nanofibers in the adhesive but without signs of fiber pull-out due to crack bridging. Therefore, it seems that the presence of a number of anchor points is enough to guarantee a fracture toughness comparable or tendentially higher than that of the virgin joint. A picture of the fracture surface of the neat adhesive (V joint) is reported in Figure 13 for the sake of comparison with Figure 12: one can see the smoother surface that essentially replicates the adherent surface, justifying a lower resistance to crack propagation. Why anchor points are very limited in this case (see example on Figure 14) is not fully understood, but it might be related to the manufacturing conditions, that include the use of spacers in order to guarantee the same thickness of the N joints. In this way, the weights applied while curing may not yield the same pressure as in the case of N joints where spacers are not present. Since keeping the same adhesive layer thickness is deemed to be essential for a proper comparison between N and V joints, an even more effective surface preparation has to be developed in order to ensure enough adhesion in all cases.

4. Conclusions

The mode I fracture toughness of a structural epoxy adhesive modified with the addition of a nylon nanomat generated by electrospinning (N joints) was evaluated by DCB testing, in comparison with that of the neat adhesive (V joints).

The nanofibers do not have shown detrimental effects on the fracture toughness of the adhesive joint, rather a trend of improvement was found, with a mechanism characterized in both N and V joints by frequent crack path deviations from one adherent to the other one, where the nanofibers seems to give a contribution to keep at least some ripples of adhesive on both sides. As failure was essentially interfacial also in V joints, it means that nanofibers did not affect the failure mechanism and, despite the etching treatment, adhesion was still not optimal. Therefore, further efforts have to be directed in future to the improvement of adhesion to understand the full potential of nanofiber as a reinforcement. At the moment, it has been demonstrated that the technique developed in this work can be used to generate pre-preg nanomats out of a structural epoxy adhesive as an alternative to more conventional carriers (e.g. glass fiber mat).

Acknowledgements

The research has been done under funding of the Regione Emilia-Romagna (POR-FESR 2014-2020),

project "TEAM SAVE –TEcnologie Abilitanti e Materiali in Soluzioni Avanzate per il Veicolo Elettrico", CUP E91B18000460007.

References

[1] da Silva, L. F. M., Oechsner, A., and Adams, R. D., *Handbook of Adhesion Technology – 2nd Ed.*, (Springer, Berlin, Germany, 2018).

[2] Kinloch, A. J., *MRS Bulletin* **28**(6), 445-448 (2003).

[3] Nemati Giv, A., Ayatollahi, M.R., Hengameh Ghaffari, S., and da Silva L.F.M., *The Journal of Adhesion* **94**(13), 1082-1121 (2018).

[4] Gupta, S.K., Shukla, D-K., and Ravindra, D.K., *The Journal of Adhesion*, DOI: 10.1080/00218464.2019.1641088 (Published online 14 July 2019).

[5] Takeda, T., and Narita, F., *Comp Sci Tech* **146**, 26-33 (2017).

[6] Burkholder, G.L., Kwon, Y.W., and Pollak R.D., *J Mater Sci* **46**, 3370–3377 (2011).

[7] Jakubinek, M.B., Ashrafi, B., Zhang, Y., Martinez-Rubi, Y., Kingston, C.T, Johnston, A., and Simard, B., *Comp B* **69**, 87–93 (2015).

[8] Gude, M.R., Prolongo, S.G., and Ureña, A., *Int J Adhes Adhes* **62**, 139–145 (2015).

[9] Korayem, A.H., Chen, S.J., Zhang, Q.H., Li, C.Y., Zhao, X.L., and Duan, W.H., *Comp B* **94**, 95-101 (2016).

[10] Khoramishad, H., and Khakzad, M., *J Adhes*, DOI: 10.1080/00218464.2016.1224184 (2016).

[11] Akpinar, I.A., Gürses, A., Akpinar, S., Gültekin, K., Akbulut, H. and Ozel, A. Investigation of mechanical and thermal properties of nanostructure-doped bulk nanocomposite adhesives, *The Journal of Adhesion* **94**(11), 847-866 (2018).

[12] Zielecki, W., Kubit, A., Trzepieciński, T., Narkiewicz, U., and Czech, Z., *Int J Adhes Adhes* **73**, 16–21 (2017).

[13] Huang, Z.M., Zhang, Y.Z., Kotaki, M., and Ramakrishna, S., *Comp Sci Tech* **63**, 2223–2253 (2003).

[14] Zucchelli, A., Focarete, M.L., Gualandi, C., and Ramakrishna, S., *Polym Adv Tech* **22**(3), 339–349 (2011).

[15] Palazzetti, R., Zucchelli, A., and Trendafilova, I., *Comp Stru* **106**, 661-671 (2013).

[16] Moroni, F., Palazzetti, R., Zucchelli, A., and Pirondi, A., *Comp B* **55**, 635-641 (2013).

[17] Giuliese, G., Palazzetti, R., Moroni, F., Zucchelli, A., and Pirondi, A., *Comp B* **78**, 384-392 (2015).

[18] Beckermann, G.W., and Pickering, K.L., *Comp A* **72**, 11–21 (2015).

[19] Saghafi, H., Palazzetti, R., Zucchelli, A., and Minak, G., *J Reinf Plast Comp* **34**(11), 907–914 (2015).

[20] Zhang, H., Bharti, A., Li, Z., Du, S., Bilotti, E., and Peijs, T., *Comp A* **79**, 116–126 (2015).

[21] Maloney, K., Fleck, N., *Int J Solids Struct* **158**, 66–75(2019)

[22] Daelemans, L., van der Heijden, S., De Baere, I., Rahier, H., Van Paepegem, W., and De Clerck, K., *Comp Sci Tech* **124**, 17-26 (2016).

[23] Daelemans, L., van der Heijden, S., De Baere, I., Rahier, H., Van Paepegem, W., and De Clerck, K., *Comp A* **94**, 10-20 (2017).

[24] Kaynana, O., Atescanb, Y., Ozden-Yeniguna, E. and Cebeci, H., *Comp B* **154**, 186-194 (2018).

[25] Oh, H.J., Kim, H.Y., and Kim, S.S., *J Adhes* **90**(9), 787-801 (2014).

[26] On, S.Y., Kim, M.S., and Kim, S.S., *Comp Stru* **159**, 636–645 (2017).

[27] Razavi, S.M.J., Esmaeely Neisiany, R., Ayatollahi, M.R., Ramakrishna, S., Nouri Khorasani, S., and Berto, F., *Theor Appl Fract Mech* **97**, 448-453 (2017).

[28] Ekrem, M., Avcı, A., *Composites Part B* **138**, 256–264 (2018).

[29] Musiari, F., Pirondi, A., Zucchelli, A., Menozzi, D., Belcari, J., Brugo, T.M., Zomparelli. L., *The Journal of Adhesion*, **94**(11), 974-990 (2017)

[30] Brugo, T.M., Musiari, F., Pirondi, A., Zucchelli, A., Cocchi, D., Menozzi, D., Proc IMechE Part L: J Materials: Design and Applications **233**(3), 465-474 (2018).

[31] Kinloch, A.J., *Adhesion and Adhesives: Science and Technology*, (Chapman & Hall, London, UK, 1987).

[32] Krenk, S., *Eng Fract Mech* **43**, 549-559 (1992).

Table 1: electrospinning process parameters

Electrospinning parameter	**EM252 nanomat**
Voltage (kV)	25
Needle inner diameter (mm)	0.51
Needle-collector distance (mm)	65
Flow rate (ml/h)	0.7
Environmental conditions (°C, %R.H.)	24, 40
Tangential speed of the collecting drum (mm/s)	400

Table 2. Bulk properties at room temperature of the two-part epoxy adhesives Elan-tech® AS46/AW46, (ELANTAS Europe srl, Italy).

Property	**Unit**	
Viscosity	mPa*s	20-32000
Gel time	h	5-6
Cure cycle suggested by the supplier	h	3
	°C	50
Glass transition temperature (ASTM D 3418) after 24 h at RT	°C	48-54
Flexural strength (ASTM D 790)	MPa	56-64
Maximum strain (ASTM D 790)	%	4.5-6.5
Strain at break (ASTM D 790)	%	> 15
Flexural modulus (ASTM D 790)	MPa	1600-2000
Tensile strength (ASTM D 638)	MPa	36-44
Elongation at break (ASTM D 638)	%	4-6
Shear strength (ASTM D 1002) on Aluminum, cured 16h at 40°C	MPa	20-25
Peel strength (ASTM D 1876) on Aluminum, cured 3h at 50°C	N/cm	48-58

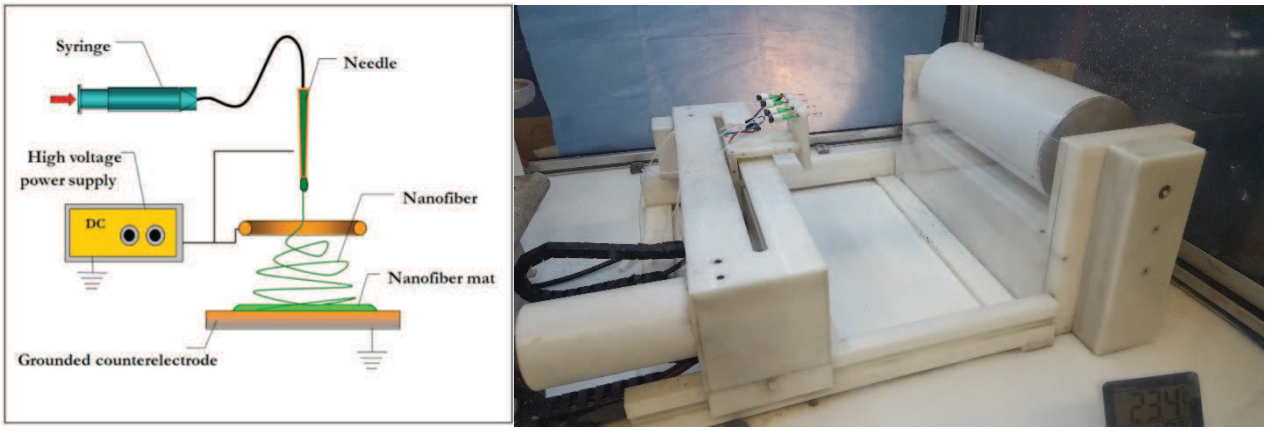

Figure 1. Outline of the electrospinning process.

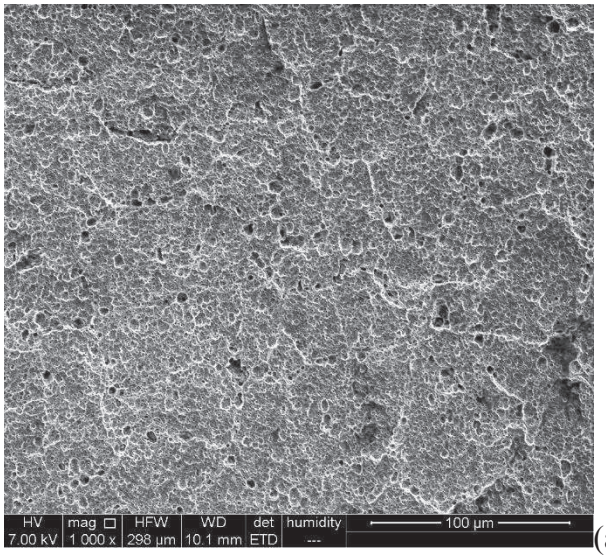

(a)
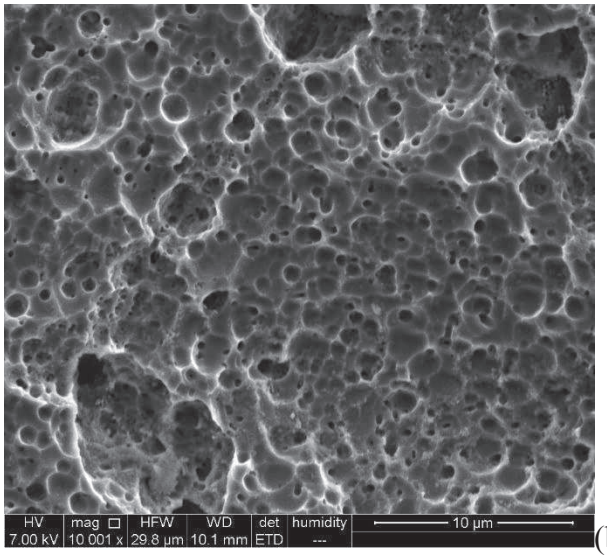

(b)

Figure 2. Surface morphology of the aluminum adherent after preparation in at 1000x (a) and 10000x (b) magnification.

External surface	Rupture surface
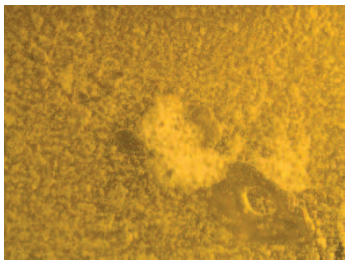	

Figure 3. Results of preliminary tests in terms of air entrapment after curing of the two-part epoxy system + nanomat, from [30].

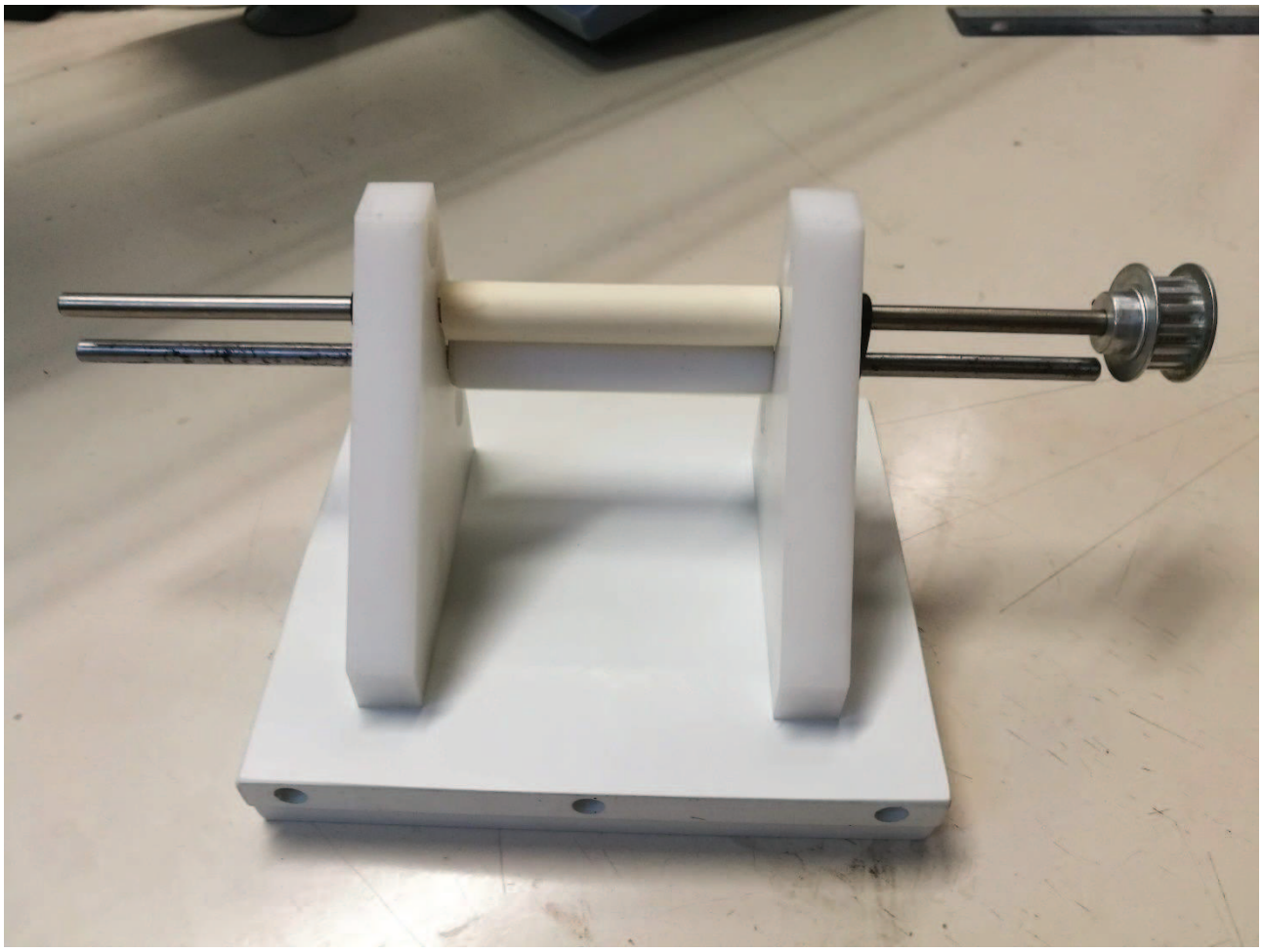

Figure 4. Calibration device based on counter-rotating drums.

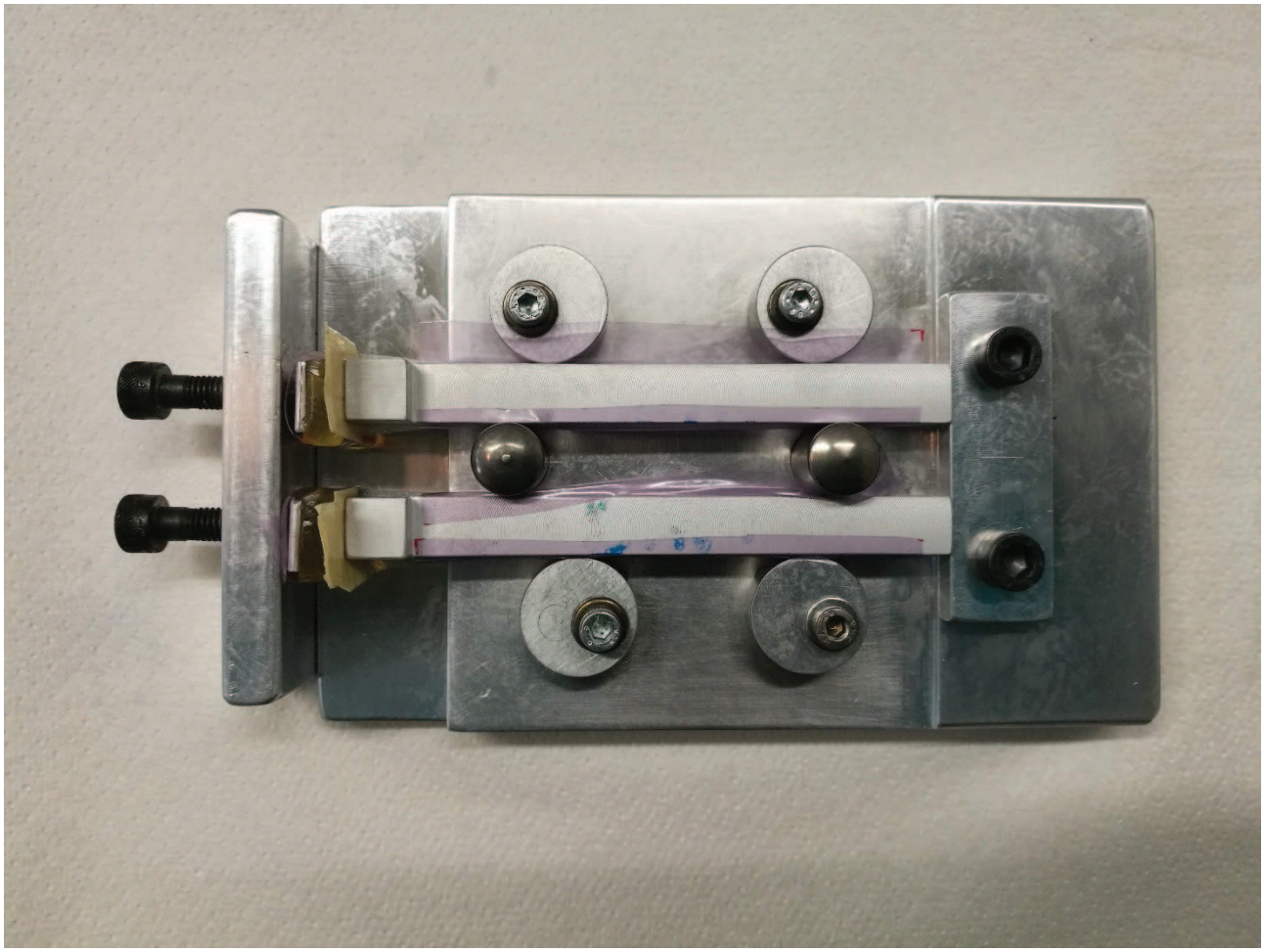

Figure 5. DCB joints placed in the template. One can notice the pink polyethylene foils wrapping the specimens in order to avoid adhesion to the template.

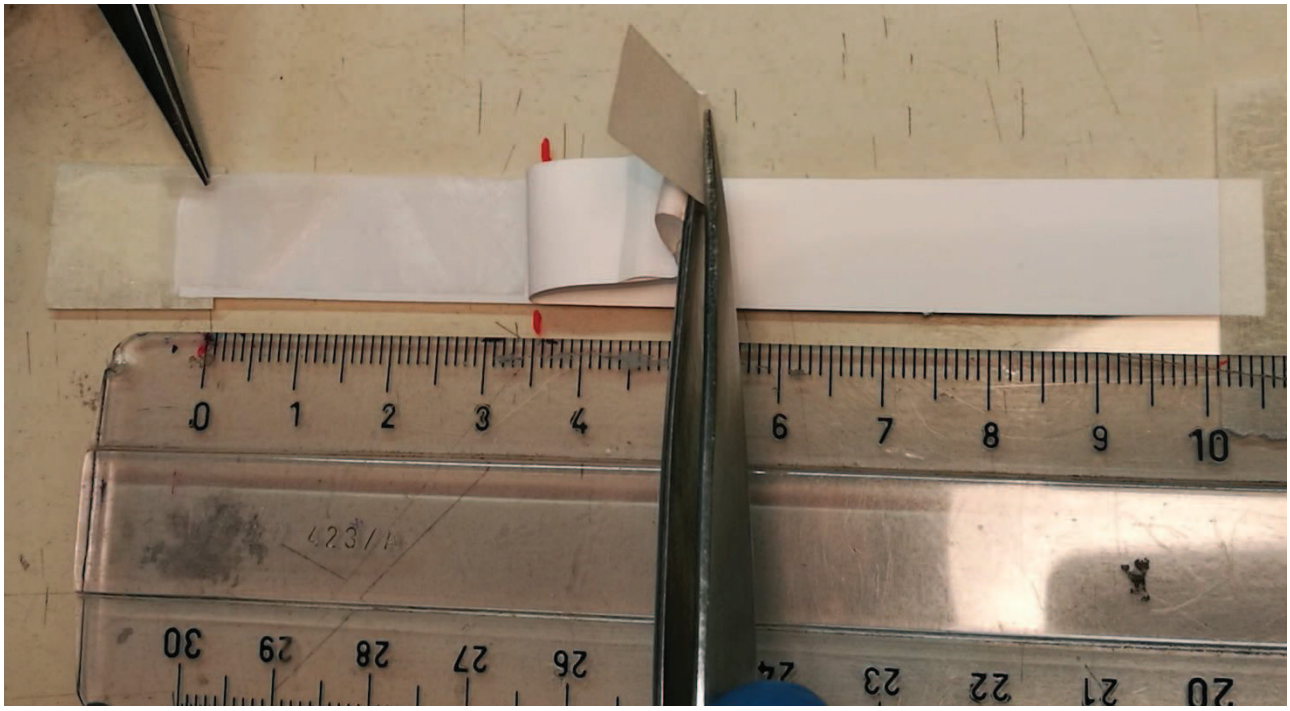

(a)

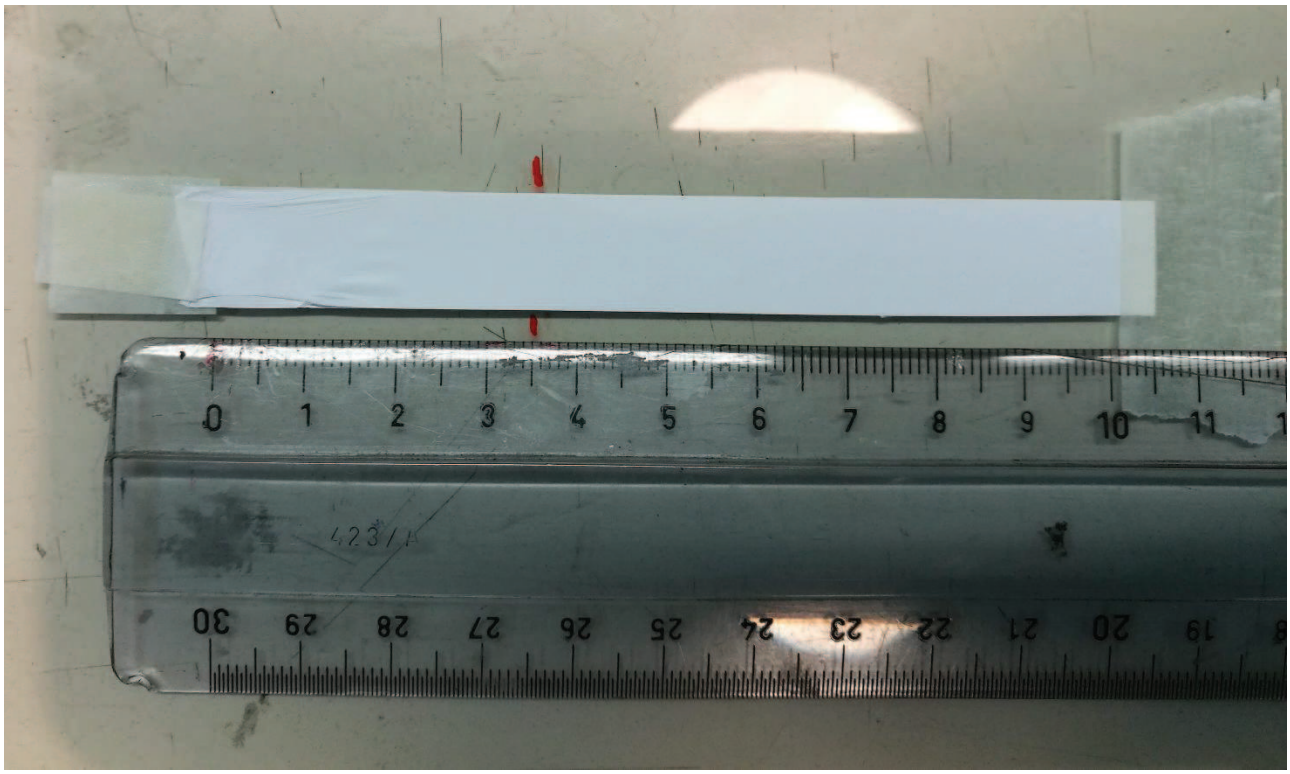

(b)

Figure 6. Illustration of precrack insertion procedure: a) exfoliation of the nanomat at one side and insertion of the teflon foil; b) precracked nanomat ready for being wet with the adhesive.

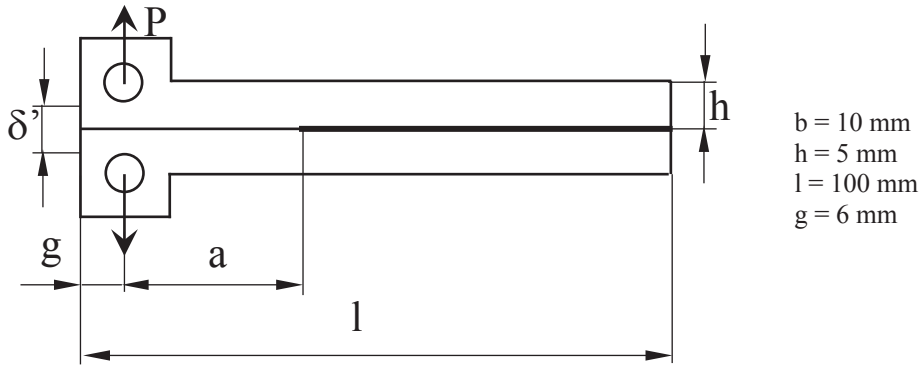

Figure 7. Outline of the DCB test setup.

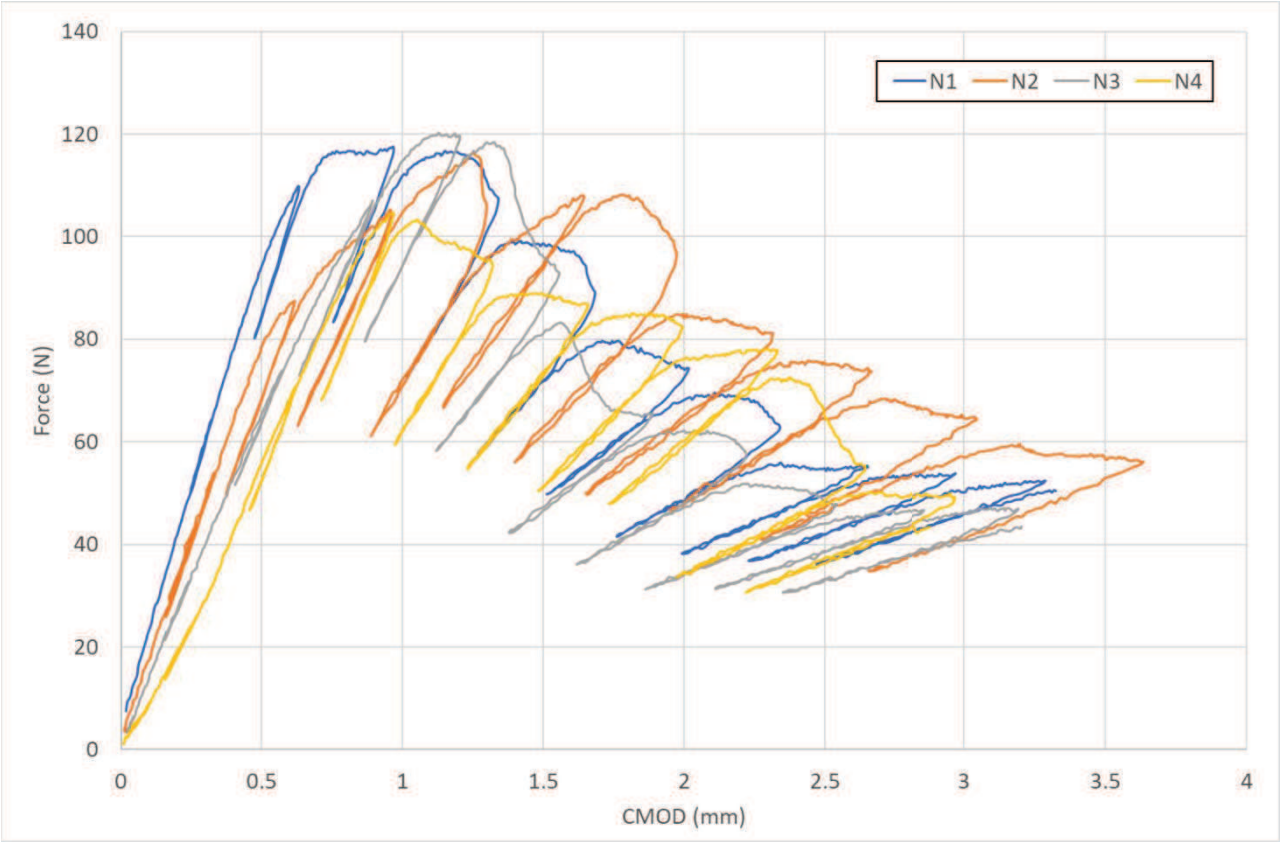

(a)

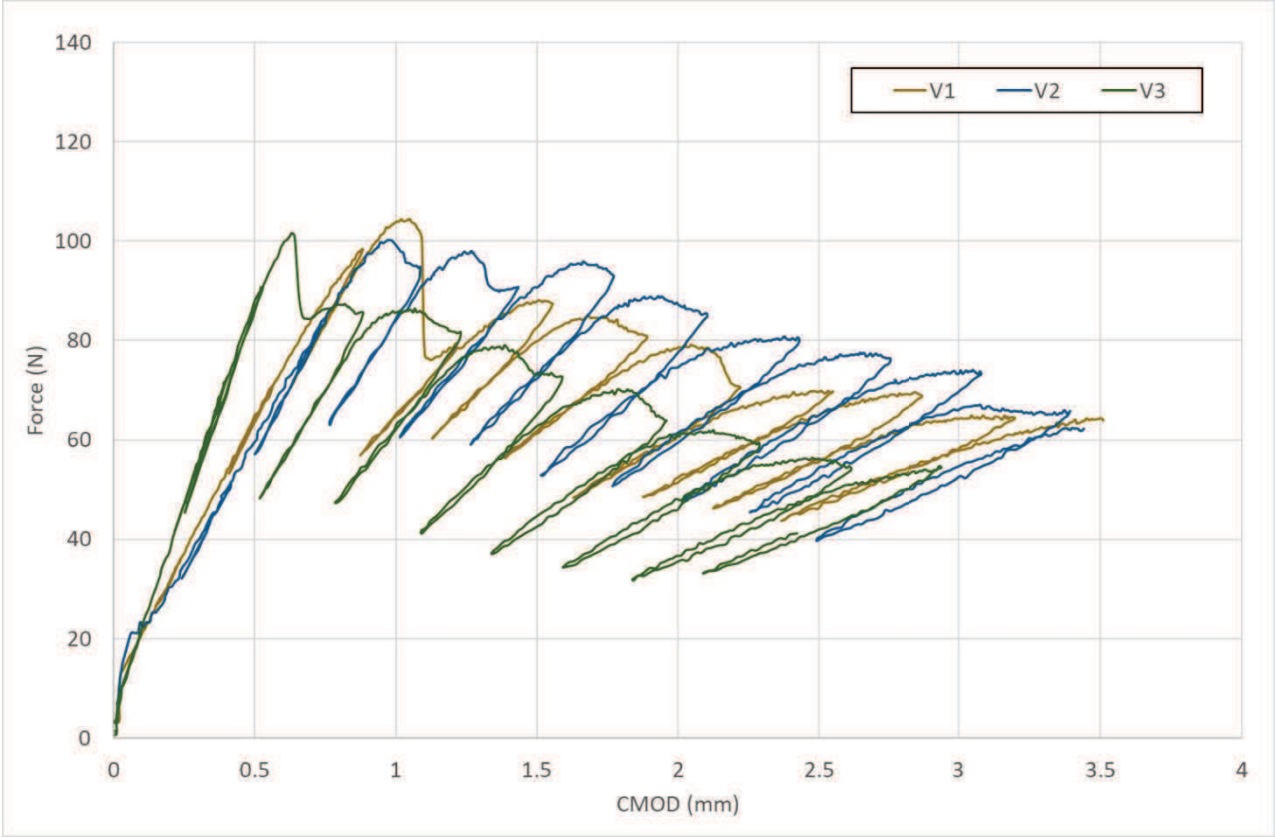

(b)

Figure 8. Force vs. CMOD od nanomodified (a) and virgin (b) DCB joints.

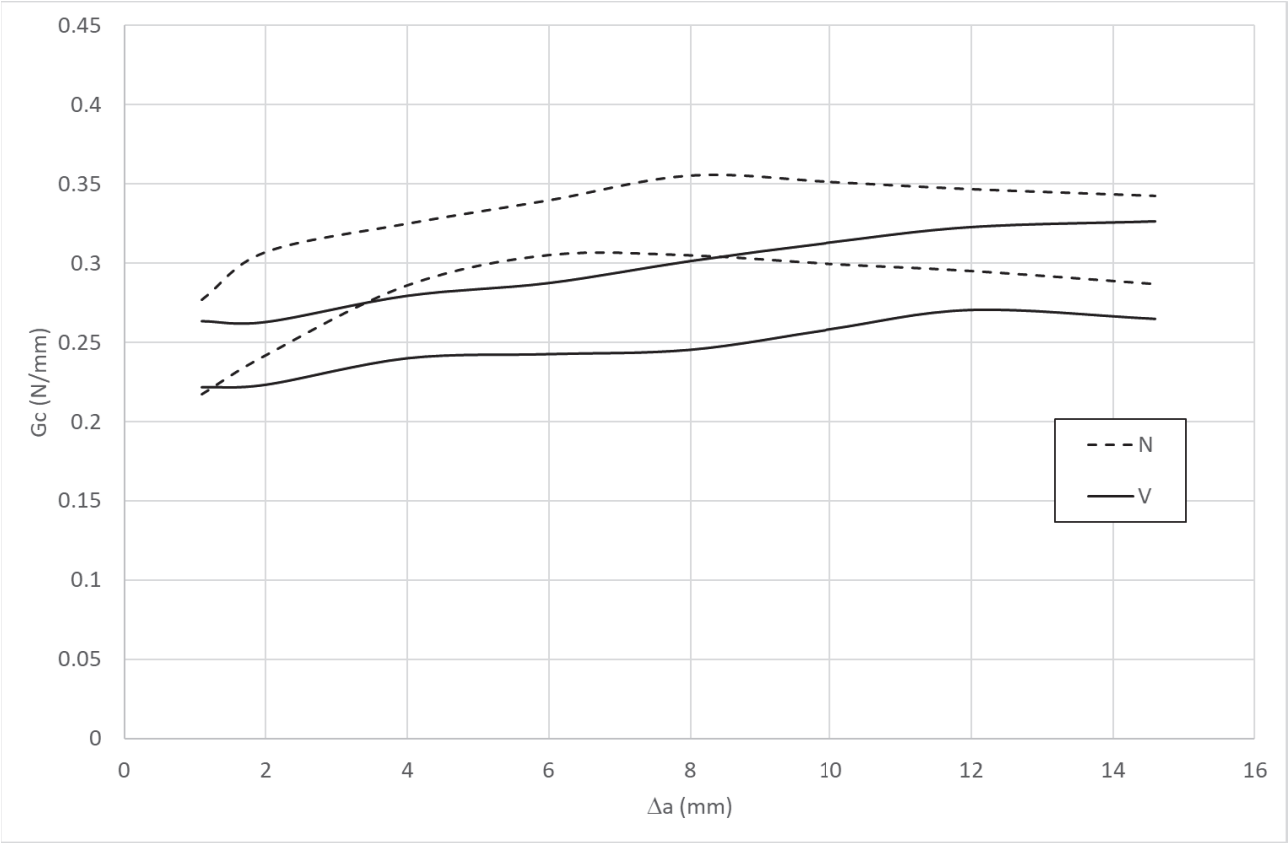

Figure 9. Fracture toughness vs. crack propagation. The lines represent the scatterband of experiments (average value +/- one-half standard deviation).

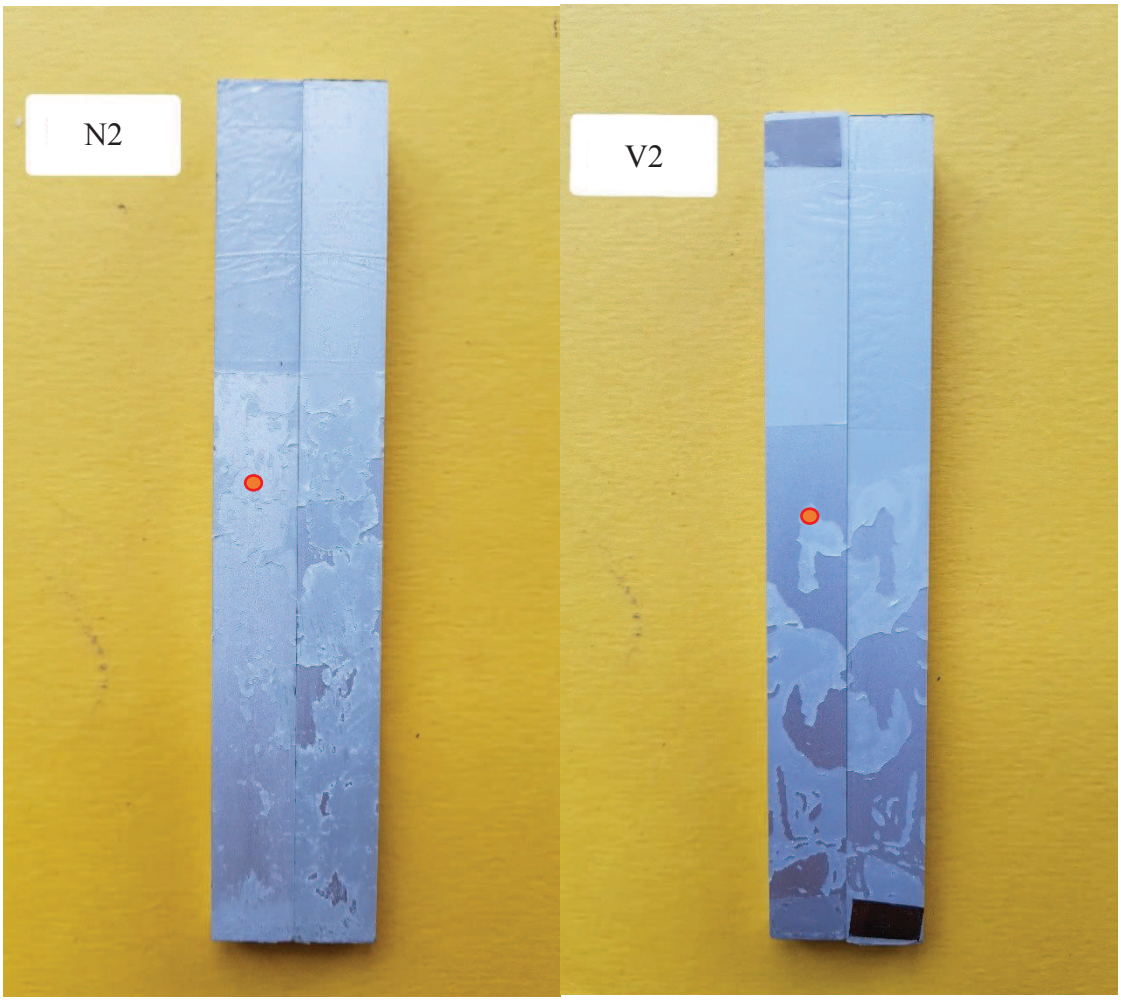

(a) (b)

Figure 10. Fracture surface of N2 (a) and V2 (b) joints. The red dots represent the position where the ESEM images in Figure 12 and Figure 13 are taken

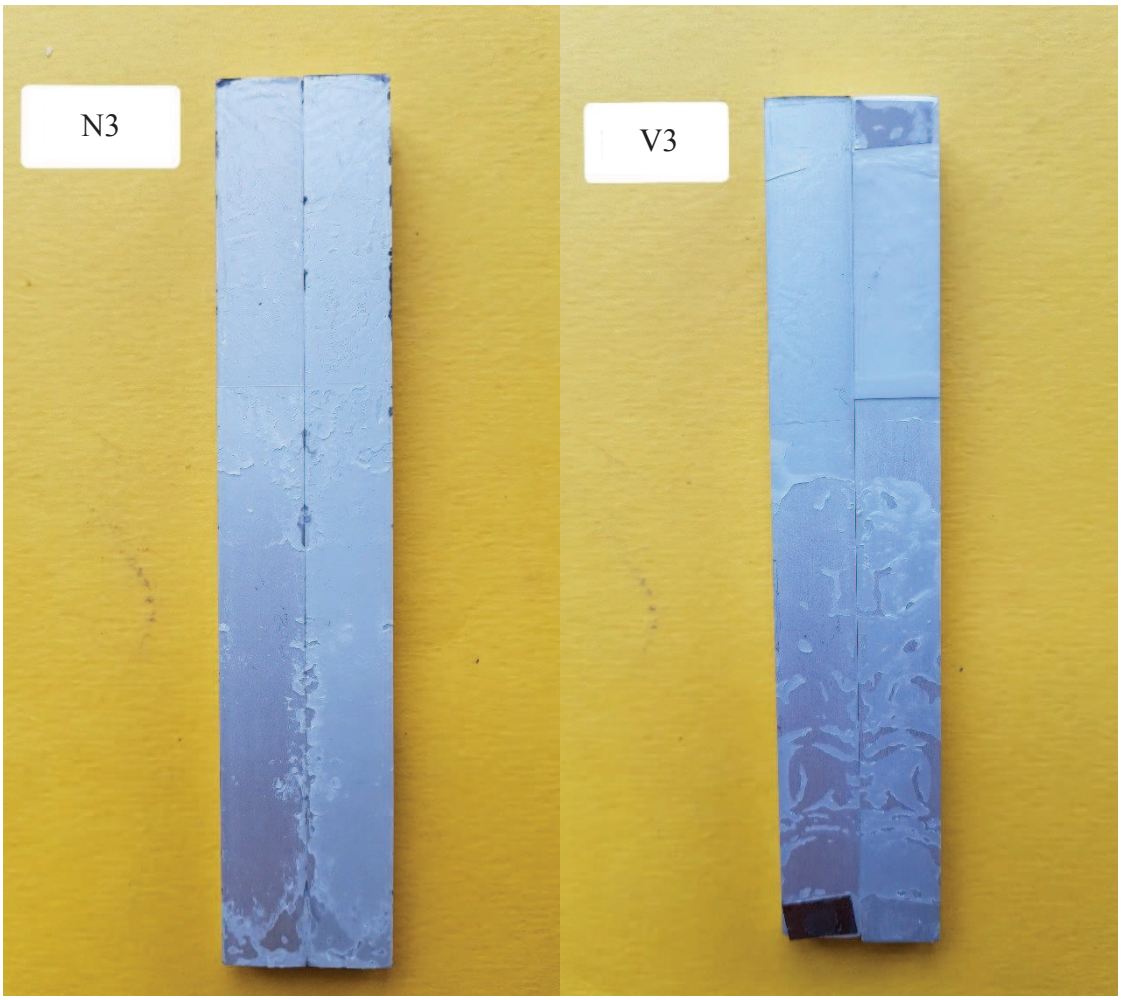

(a) (b)

Figure 11. Fracture surface of N3 (a) and V3 (b) joints.

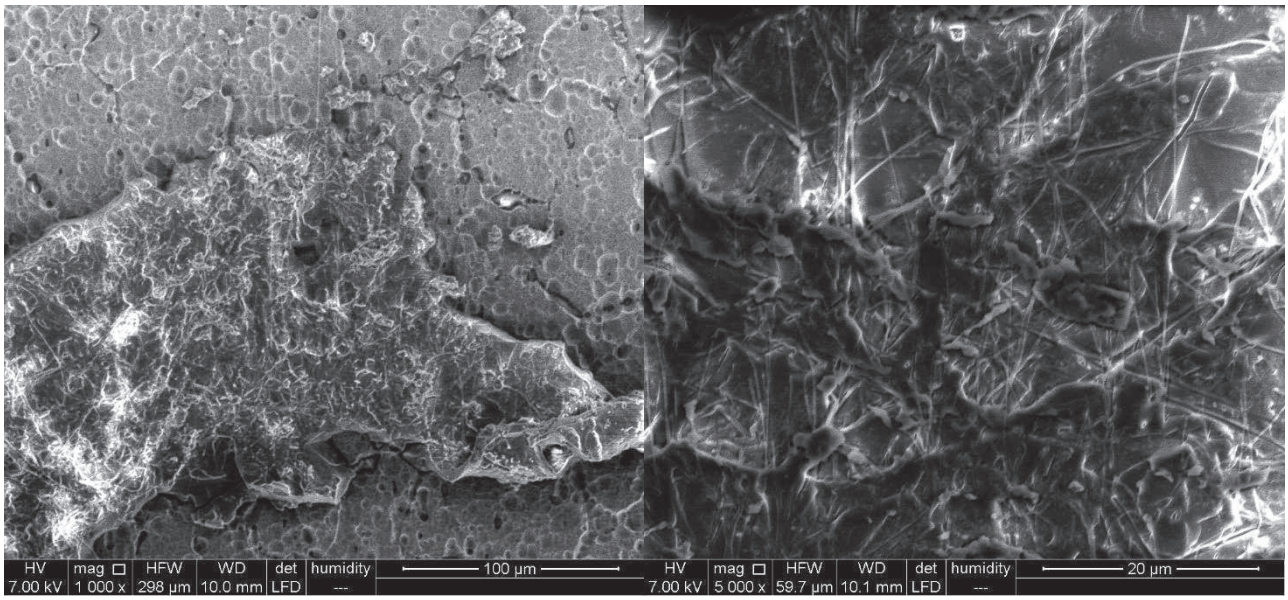

(a) (b)

Figure 12. ESEM image of the fracture surface of a N specimen at 1000 x (a) and 5000 x (b) magnification.

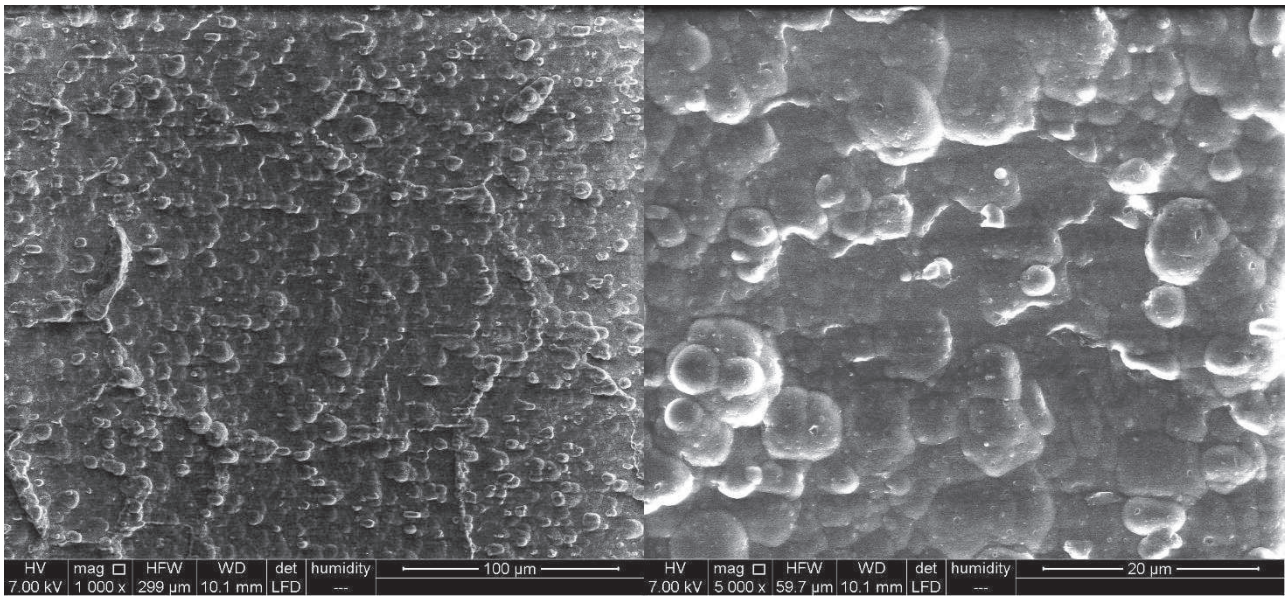

Figure 13. ESEM image of the fracture surface of a V specimen (adhesive side) at 1000 x (a) and 5000 x (b) magnification.

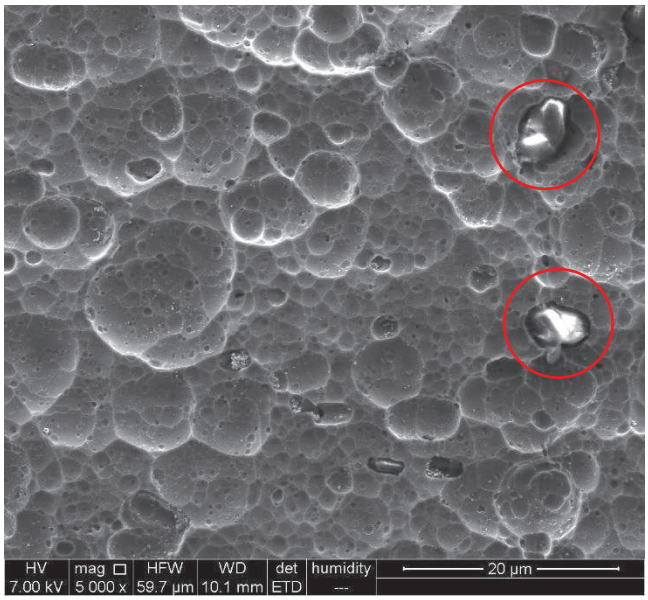

Figure 14. ESEM image of the fracture surface of a V specimen (adherent side) at 5000 x magnification, showing a few adhesive leftovers entrapped in surface pits (circled in red).